

Enhancing Graphitic Carbon Precursors from Coal Pyrolysis: A Comparative Analysis of Microwave Plasma and Conventional Thermal Upgradation Methods

Akshay Gharpure* and Randy L. Vander Wal

Cite This: *ACS Omega* 2023, 8, 40587–40599

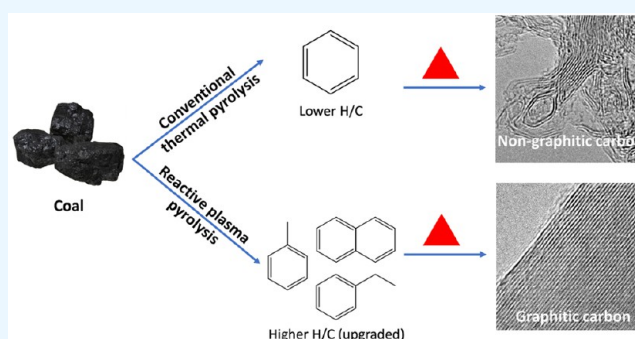
Read Online

ACCESS |

Metrics & More

Article Recommendations

ABSTRACT: This study investigates and compares the efficacy of conventional thermal pyrolysis and microwave (MW) plasma pyrolysis in upgrading coal-derived precursors. Coal samples presenting a range of ranks were pyrolyzed under various reactive and nonreactive atmospheres using a pyroprobe, with the pyrolyzates analyzed by gas chromatography–mass spectrometry (GC–MS). Comparative MW plasma tests were conducted using a modified countertop MW unit, with condensed products similarly analyzed by GC–MS. A predominant coal devolatilization product—benzene was selected for analyzing the reactive MW plasma upgradation. Results demonstrate that conventional thermal pyrolysis lacks effectiveness in upgrading the precursors. To gain insight into the underlying reasons, chemical kinetic simulations were conducted. Oppositely, reactive MW plasma pyrolysis demonstrated remarkable precursor upgradation. These condensed MW plasma pyrolysis products were then subjected to a carbonization and graphitization heat-treatment with a comprehensive graphitic quality assessment conducted using X-ray diffraction and transmission electron microscopy. After graphitization, the MW plasma-upgraded precursor produced a carbon with a crystallite size several times greater than that of the initial benzene. By MW plasma processing, the poorly graphitizable benzene precursor was transformed into a highly graphitizable precursor comparable to coal tar pitch. The underlying reasons for this significant improvement were investigated by analyzing the compositional changes in the precursor under various reactive environments.



1. INTRODUCTION

Advanced composite materials, whether carbon-based or polymer-based matrix, rely upon carbon fibers for reinforcement and electrical and thermal conductivity. The mechanical,^{1–4} thermal,^{5,6} and electrical^{5,7} properties of carbon materials are governed by their graphitic quality, which is precursor-dependent. Coal tar (CT) and pitch are excellent low-cost precursors for carbon fibers and as feedstock for carbon-based materials.^{8–11} Domestic sources for CT are declining.^{12,13} CT is produced by coking coal, i.e., devolatilizing under an inert atmosphere.¹⁴ Notwithstanding these factors, traditional methods of extracting CT also have limitations in terms of product yield, quality, and environmental impact. Conventional thermal pyrolysis of coal leads to a lower yield and quality of the product due to secondary cracking reactions. Similar challenges are also associated with the thermal pyrolysis of biomass.¹⁵ These factors motivate the study of microwave (MW)-driven plasma-assisted pyrolysis for the extraction of volatiles from coal. Energy efficiency is a dramatic advantage of MW heating—industrial-scale magnetrons demonstrate about 80% energy efficiency at output power on the order of 100 kW.¹⁶ A key

innovation is the ability to process coal with little to no CO₂ emissions or water consumption. In addition to these green advantages, MW plasma pyrolysis under a reactive atmosphere has the potential to improve the product by increasing its hydrogen content. In an Ar atmosphere containing H₂ or CH₄, under high-power MW irradiation, dissociation occurs, forming H atoms and methyl radicals. These species are capable of capping radicals by hydrogenation and methylation reactions—suppressing both retrogressive and secondary cracking reactions¹⁷ that are typical of the conventional pyrolysis processes and decrease liquid and tar yields.¹⁸ Such capping reactions by H atoms and methyl radicals also lead to the upgrading of unsaturated and aromatic compounds. In this work, the term

Received: July 24, 2023**Accepted:** September 14, 2023**Published:** October 18, 2023

Table 1. Thermal Pyrolysis Test Matrix

coal sample	particle mesh size	temp ramp rate (°C/ms)	final temperature	gas	purpose
APCS-2	−20	10	610	Ar	to verify and compare with the py-gc-ms data available in the literature
APCS-3	−20	10	610	Ar	to verify and compare with the available py-gc-/ms data available in the literature
APCS-5	−20	10	610	Ar	to verify and compare with the available py-gc-/ms data available in the literature
APCS-8	−20	10	610	Ar	to verify and compare with the available py-gc-/ms data available in the literature
APCS-3	−100	10	1000	Ar	final temperature effect
APCS-5	−100	10	1000	Ar	final temperature effect
APCS-5	−20	10	1000	Ar	particle size effect
DECS-19	−20	10	1000	Ar	temperature ramp rate and coal rank effect (inert benchmark)
DECS-19	−20	20	1000	Ar	temperature ramp rate and coal rank effect (inert benchmark)
DECS-19	−20	1	1000	Ar	temperature ramp rate and coal rank effect (inert benchmark)
DECS-6	−20	1	1000	Ar	temperature ramp rate and coal rank effect (inert benchmark)
DECS-19	−20	1	1000	50% CH ₄ –50% Ar	effect of CH ₄
DECS-19	−20	1	1000	50% H ₂ –50% Ar	effect of H ₂
DECS-6	−20	1	1000	50% CH ₄ –50% Ar	effect of CH ₄
DECS-6	−20	1	1000	50% H ₂ –50% Ar	effect of H ₂
DECS-19	−20	1	1000	25% CH ₄ –25% H ₂ –50% Ar	effect of CH ₄ –H ₂
DECS-6	−20	1	1000	25% CH ₄ –25% H ₂ –50% Ar	effect of CH ₄ –H ₂
DECS-19 char	−20	1	1000	50% CH ₄ –50% Ar	effect of char catalysis

“upgradation” is used to indicate an increase in the hydrogen-to-carbon ratio (H/C).

Extensively studied for product yield as a function of coal rank, temperature ramp, and final temperature, the conventional thermal pyrolysis approach has been thoroughly reviewed elsewhere.^{19–23} To date, MW pyrolysis of virgin coal has been largely applied to other coal processing purposes, such as drying, rather than devolatilization.^{24–28} Prior studies on MW pyrolysis have been carried out for select ranks of coal with a focus on total yield rather than product distribution.^{23,29,30} Furthermore, there have been limited studies of MW-driven pyrolysis under reactive gases. A recent study by Singh et al. highlighted increased oil yield by MW processing coal under a reactive CH₄ atmosphere.³¹ With Pittsburgh-8 coal, more than a 100% increase in oil yield compared to benchmark (thermal) testing was measured, with nearly a 4x increase in oil yield from Black Thunder coal. Yang et al. demonstrated the potential of increasing the H/C ratio through radical capping, albeit with the use of catalysts, to activate methane for low-temperature reactions with coal.³² Demonstrating increased yield, Kamei et al. reacted brown coal with methane under MW radiation³³ and speculated that reactive radicals are generated from methane under MW plasma, which undergoes a complicated set of reactions with coal. Meanwhile, Rahimi et al. created a He/CH₄ plasma in a MW discharge, forming reactive methyl radicals, ultimately for upgrading heavy oils and bitumen but initially using toluene as a model compound.³⁴ Beside hydrogenation products, the addition of methyl radicals to toluene produced substituted toluene and ethylbenzene, thereby demonstrating upgrading by improving H/C content. However, these studies lacked a comparison with baseline results of thermal pyrolysis, hydrogen, and nonreactive plasma environments, thereby failing to identify the distinguishing characteristics between the reaction drivers and associated species. Thus, it is difficult to assess the differences in product distributions under different reactive environments in these prior studies of MW pyrolysis.

Beyond upgrading, the graphitization potential of upgraded precursors has not been studied before. This article is aimed at comparing the effectiveness of MW plasma pyrolysis with conventional thermal pyrolysis for upgrading of coal-derived precursors and the resultant potential improvements in graphitizability.

2. EXPERIMENTAL METHODOLOGY

2.1. Py-GC–MS.

Pyrolysis-gas chromatography–mass spectrometry (py-GC–MS) generates volatile products from thermal decomposition, which are separated by gas chromatography and identified from their mass spectra. A pyroprobe provides a convenient means to achieve rapid pyrolysis of a small coal sample, which has the advantage of not overloading the GC–MS and minimizing any selective detection due to otherwise required high split ratios. With a lower sample quantity, the time for tars to escape from the matrix is also minimized, avoiding potential secondary and surface reactions of liberated tars.

The CDS 6200 pyroprobe consists of a platinum filament that wraps around a quartz capillary and pyrolyzes the sample at any temperature ramp from 0.01 to 20 °C/ms to a final temperature of up to 1300 °C. Samples can be pyrolyzed in an inert or reactive environment by passing the desired gas stream through the quartz capillary tube holding the pyrolyzing coal sample. The pyrolysis products swept by the gas stream were cryotrapped and then sent to a Thermo Scientific TSQ Triple Quad 9000 GC/MS system. Argonne premium coal samples (APCS) representing a range of ranks—APCS-2: Wyodak (subC), APCS-3: Illinois #6 (hvCb), APCS-5: Pocahontas no. 3 (lvb), and APCS-8: Beulah (ligA)—were used for verification of the py-GC/MS system by comparing results with the sample bank database.³⁵ DECS-6 and DECS-19 were selected for the fast thermal benchmarking experiments in inert as well as reactive environments. These tests used a temperature ramp rate of 1 °C/ms up to a final temperature of 1000 °C and a hold time of 3 s to ensure

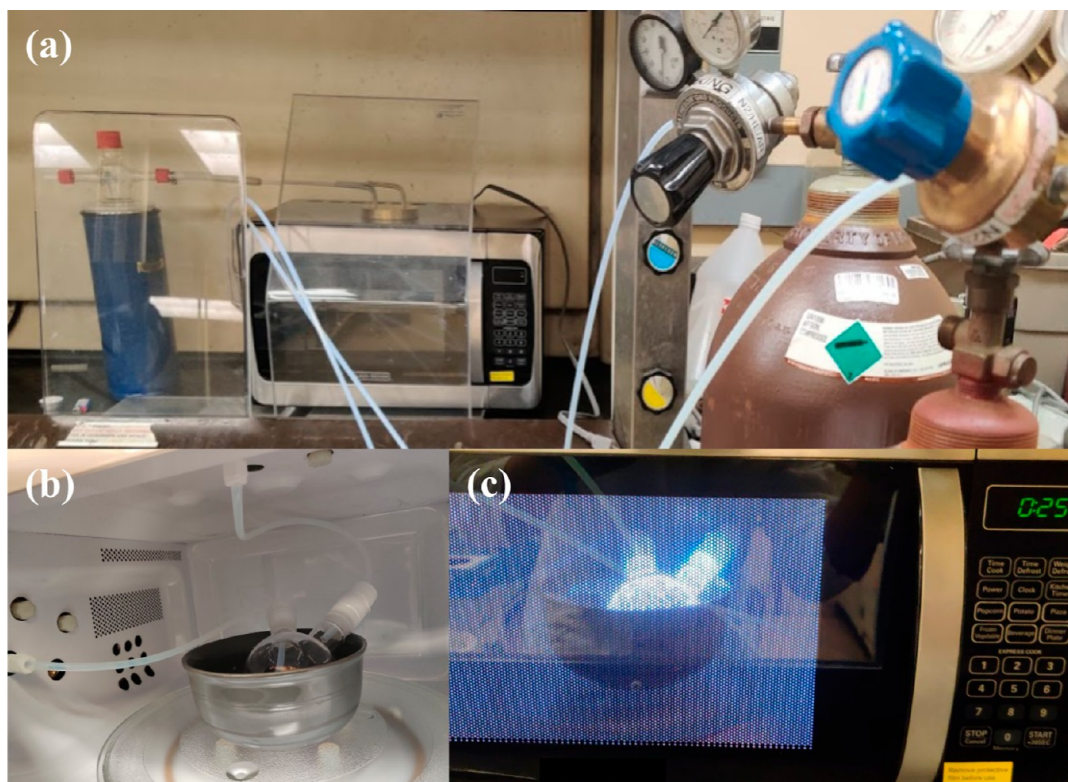


Figure 1. Images showing (a) MW plasma setup, (b) inside connections, and (c) active plasma during operation.

complete expulsion of volatiles. Additional tests were also included to assess the effect of particle size, gas flow rate, temperature ramp rate, and final temperature hold time.

Table 1 shows the GC–MS test matrix used for fast thermal pyrolysis studies. Compounds corresponding to each peak in the pyrograms were identified by matching the associated mass spectra with the NIST mass spectral library. Quantification for each identified species was performed by normalizing the integrated area of that peak to the total area of all peaks.

2.2. CHEMKIN Simulations. Chemical kinetic simulations were run to test reactions and volatile upgrading under fast thermal conditions. A detailed soot mechanism with 500+ species and 25,000+ reactions developed by the CRECK modeling group^{36,37} was used with a plug-flow reactor (PFR) model. Various model compounds like benzene–toluene–xylene (BTX), naphthalene, methylnaphthalene, cyclohexane, and *n*-decane were reacted for 0.125, 1 and 5 s residence time under the inert and reactive environment in a PFR maintained at 1000 °C. The concentration of model compounds used was 1% within a balance of inert plus desired reactive component(s). These conditions were approximated by considering the dimensions of the quartz capillary, sample amount, and flow rate of the gas in the py-GC-MS setup. Heating rates, final temperatures, and hold times were varied according to the py-GC-MS conditions.

2.3. MW Plasma Tests Using Modified MW. A laboratory MW plasma setup was developed to conduct comparative MW plasma conversion tests. Several holes were drilled into an ordinary countertop MW to feed reactants and collect reacted precursor products. The turntable was retained but lifted with a polytetrafluoroethylene (PTFE) support to prevent it from turning. PTFE tubes carry the gases in and out of a three-necked quartz flask acting as a reactor, with PTFE-holed stoppers

sealing the reactor. Steel mesh is used in the reactor as a plasma initiator. When the MW is turned on, sparks initiate a uniform blue corona discharge inside the reactor, which is sustained while the MW is on. The surrounding volume outside the reactor (yet in the MW) is continuously flushed with inert N₂. For precaution, the runs were conducted in a fume hood, and an additional plexiglass shield was used for safety. Inert gas was fed into the MW using one of the access holes to maintain an inert environment outside the quartz reactor for added safety. Figure 1 shows images of the setup and active MW plasma.

As a primary coal devolatilization product observed in py-GC-MS, benzene was selected as a model compound with which to test reactive MW plasma upgrading. A small amount of benzene vapors was reacted in different MW plasma environments: inert (pure Ar) and reactive (50% CH₄–50% Ar and 50% H₂–50% Ar). The precursor products were condensed outside the MW in a cold trap. The flow rates were maintained to have the residence time in the reactor the same as in the thermal py-GC-MS tests. The process was repeated in multiple batches to collect enough samples for analysis and further heat treatment (HT). The products of benzene exposed to MW plasma in pure Ar, 50% H₂–50% Ar, and 50% CH₄–50% Ar are hereafter designated as ap-benzene, hp-benzene, and mp-benzene, respectively. To identify differences between major product species derived from the reaction of benzene in various MW plasma environments, these products were further analyzed using an Agilent 7890A GC coupled with an Agilent 5975 MS.

2.4. Study of Model Compounds. The potential for improving graphitic quality by upgrading precursors, i.e., by increasing the H/C ratio, was tested using model polyaromatic hydrocarbons (PAHs) versus their methylated and hydrogenated versions as precursors. Naphthalene and anthracene were selected as being commonly available and the primary

products of coal devolatilization processes. Methylanthracene and methylanthracene were selected as the model compounds with methylation, while dihydronaphthalene represented upgradation via hydrogenation.

2.5. Carbonization and Graphitization. All samples have been carbonized at 600 °C for 3 h under inert using a Thermolyne 21100 tube furnace. The samples were loaded in combustion boats and inserted in a horizontal tube furnace containing an alumina tube. The furnace was continuously purged with nitrogen to maintain an inert atmosphere. A sealed tubing reactor setup was required for carbonizing highly volatile samples (model compounds and MW-upgraded products), which escape and give no solid carbon yield in the open boat setup. The sealed tubing reactors were purged of air with compressed nitrogen through the quick-connect manifold. The obtained cokes were subsequently graphitized (GR) at 2500 °C for 1 h in a Centorr series 45 graphitization furnace. Air was removed from the graphitization furnace by three sequenced pump-down cycles (to less than 100 mL), each followed by an argon backfill.

2.6. Material Characterization. **2.6.1. TEM.** Transmission electron microscopy (TEM) uses a beam of highly energetic electrons that transmit through the specimen to form a highly magnified image. The images were taken by using an FEI Talos F200X scanning/transmission electron microscope equipped with an FEG source providing 0.12 nm resolution. The TEM samples were prepared by sonicating a small amount of ground material in ethanol and drop-casting it on a 300 mesh C/Cu lattice TEM grid. The instrument was operated at 200 kV, and the samples were imaged at various magnifications in the range of 10 to 500 kX. Selected area electron diffraction (SAED) patterns were obtained to assess the local crystallinity of an individual flake/particle.

2.6.2. XRD. X-ray diffraction (XRD) was used for assessing the bulk graphitic quality of the heat-treated samples. A Malvern PANalytical Empyrean diffractometer equipped with a Cu source ($\lambda = 1.54 \text{ \AA}$), para-focusing optics, and a PIXcel 3D detector for all measurements. The spectrum was scanned in the 2θ range of 5–90°. Peak deconvolution and quantification were performed using MDI JADE, and the lowest residual fits were taken for postprocessing. The in-plane crystallite diameter (L_a) and stacking height (L_c) were determined by applying the Scherrer equation, utilizing K_a and K_c values of 1.84 and 0.89, respectively.

2.6.3. FTIR. Fourier transform infrared (FTIR) spectroscopy was used here for the characterization of the aromaticity of the tars based on the absorption of IR radiation. Bruker Vertex 70v equipped with a liquid nitrogen-cooled mercury–cadmium–telluride detector was used to collect FTIR spectra in the ATR mode of samples. The aromaticity index of the pitches was calculated from the analysis of the aromatic hydrogen band around 3050 cm^{-1} and the aliphatic hydrogen band around 2920 cm^{-1} . A linear background was subtracted from each peak region, and the aromaticity index was calculated from the integrated peak areas as
$$\frac{(\text{peak area})_{3050 \text{ cm}^{-1}}}{(\text{peak area})_{3050 \text{ cm}^{-1}} + (\text{peak area})_{2920 \text{ cm}^{-1}}}$$

3. RESULTS

3.1. Thermal Upgradation Benchmark Using Py-GC–MS. For the verification test, the identified peaks were manually grouped into compound classes: aliphatics, phenols, and nonoxygenated PAHs. These results correlated well with the sample bank database³⁵ to a first approximation. Although lower

than expected aliphatic products were observed, the results are in general agreement with the best-observed correlation in the reference study finding, with decreasing phenolic products with increasing rank. Notably, many peaks remained unidentified in the reference database, likely because of the coelution problem resulting in overlapping peaks and lack of spectral recognition in 1998. With improved instrumentation and the availability of more mass spectral profiles for reference, our data, in some sense, represent more accurate volatile identification from these coals. Table 2 shows compound classification for APCS coals

Table 2. Compound Classification from Py-GC/MS to 610 °C Inert at 10 °C/ms

compound class	APCS-2	APCS-3	APCS-5	APCS-8
alkanes and alkene	29.8	7.3	4.9	16.7
phenols	25.5	28.9	2.8	30.1
nonoxygenated PAHs	44.7	63.8	92.3	53.2

pyrolyzed to 610 °C in an inert state at 20 °C/ms from py-GC–MS tests. Increasing the final temperature from 610 to 1000 °C substantially increased the BTX yield while at the same time decreasing oxygenated PAHs, as shown in Table 3. This effect was more prominent for APCS-3 (hvCb) than for APCS-5 (Ivb).

The product composition showed minimal variation when the heating ramp rate was altered between 1, 10, and 20 °C/ms, as shown in Table 4. Changing the particle size (not shown here) of the coal, ranging between –20 and –100 mesh, yielded a very similar composition, which gives confidence that slight differences in the individual particles were not critical. Figure 2 shows an overlay of total ion chromatograms of DECS-19 pyrolyzates under different inert and reactive gas environments, and Table 5 provides a summary of major devolatilized species for each reaction condition. The BTX yields obtained from DECS-19 pyrolysis under different gas compositions, namely, argon, 50% CH₄–50% argon, 50% H₂–50% argon, and 25% CH₄–25% H₂–50% argon, were found to be 20.67, 24.57, 22.57, and 21.6%, respectively. The presence of CH₄ marginally improved the BTX yield, while the BTX yield for the other reactive gas mixtures was found to be comparable to that observed under inert argon conditions. The yield of methylated and hydrogenated compounds was comparable under all gas conditions, with the major product species also being identical. The fast thermal tests on both DECS-19 and DECS-6 (not shown here) under inert and reactive environments containing H₂, CH₄, and H₂ + CH₄ showed no significant differences in pyrolyzed products. This null result demonstrates the ineffectiveness of a conventional thermal treatment under a reactive environment for upgrading of precursors.

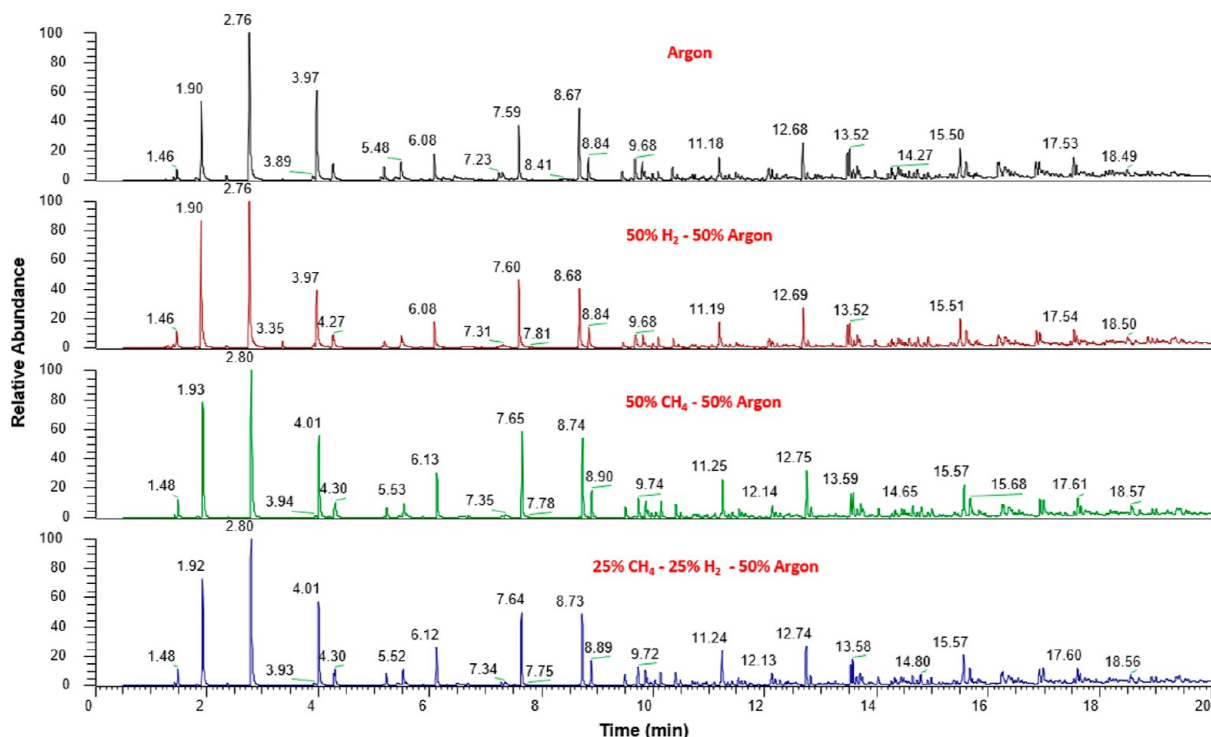
3.2. Chemical Kinetics of Thermal Upgradation. Figure 3 shows the CHEMKIN simulation results for the extent of thermal cracking and the extent of reaction of model compounds in the Ar–CH₄ environment. These revealed that there is very little thermal dissociation (<0.5%) of the reactive gases (H₂ and CH₄). Tables 6 and 10 give product composition normalized to reaction extent (i.e., excluding unreacted inputs from the products). Cyclohexane and *n*-decane crack entirely into light gases (not shown here). A maximum of only 2% benzene reacted in the Ar–CH₄ environment of which only about 8% upgraded to toluene, while most of the products were light gases due to cracking. All the model compounds reacted more in the Ar–H₂ environment but primarily generated cracked products instead of upgrading. Simulations for toluene and methylanthracene

Table 3. Major Products from Pyrolysis of APCS Coals Are Inert at Different Final Temperatures and at 10 °C/ms

APCS-3 610°C		APCS-3 1000°C		APCS-5 610°C		APCS-5 1000°C	
major product species	% conc. excluding unreacted species	major product species	% conc. excluding unreacted species	major product species	% conc. excluding unreacted species	major product species	% conc. excluding unreacted species
benzene	0.63	benzene	5.42	Benzene	2.79	benzene	6.03
toluene	1.74	toluene	5.34	Toluene	9.76	toluene	11.41
xylene	1.18	xylene	2.62	Xylene	5.25	xylene	5.83
methyl-phenol	8.94	methyl-phenol	5.96	methyl-naphthalene	2.59	methyl-naphthalene	4.93
dimethyl-phenol	5.6	dimethyl-phenol	3.09	dimethyl-naphthalene	2.62	methyl-anthracene	5.74
methyl-benzenediol	2.89	methylpropyl-benzene	2.57	trimethyl-benzene	2.43	methylene-indene	3.36
catechol	2.57	methyl-naphthalene	2.49	methyl-anthracene	2.4	methyl-fluoranthene	3.29
phenol	1.78	methylphenyl-acetylene	2.36	trimethyl-pyrene	2.4	dimethyl-pyrene	3.82
ethyl-catechol	1.11	phenol	1.03	methyl-phenol	1.5	chrysene	2.18

Table 4. Major Products from –20 Mesh DECS 19 Pyrolysis under Inert Conditions at 1000 °C with Different Ramp Rates

1°C/ms		10°C/ms		20°C/ms	
major product species	% conc. excluding unreacted species	major product species	% conc. excluding unreacted species	major product species	% conc. excluding unreacted species
benzene	4.75	benzene	5.23	benzene	5.51
toluene	9.92	Toluene	10.39	toluene	10.34
xylene	6.0	Xylene	5.12	xylene	5.18
methyl-anthracene	4.05	methyl-anthracene	4.76	methyl-anthracene	4.66
chrysene	2.56	Chrysene	3.94	chrysene	2.44
methyl-naphthalene	4.66	methyl-naphthalene	3.54	methyl-naphthalene	4.68
methyl-fluoranthene	3.27	methyl-fluoranthene	3.25	methyl-fluoranthene	3.62
methylene-indene	2.73	methylene-indene	2.92	methylene-indene	3.06
dimethyl-naphthalene	2.27	dimethyl-naphthalene	1.36	dimethyl-naphthalene	1.34
phenanthrene	2.28	phenanthrene	2.4	phenanthrene	2.0
ethylbenzene	1.67	ethylbenzene	1.77	ethylbenzene	1.61

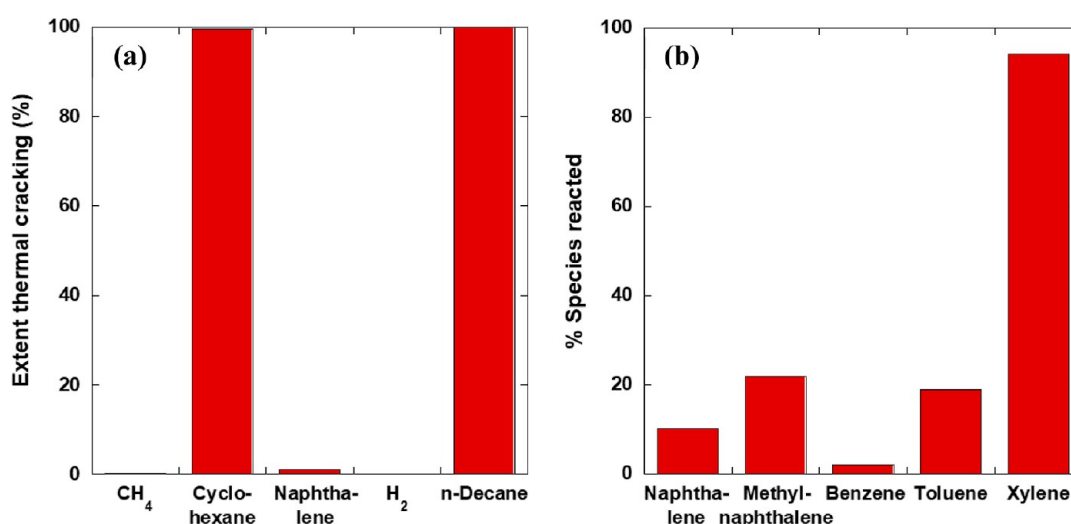
**Figure 2.** Total ion chromatograms of DECS-19 pyrolyzates under different inert and reactive gas environments.

showed that the addition of another $-\text{CH}_3$ or $-\text{H}$ to the aromatic compounds under these reaction conditions was even

lower. In the $\text{Ar}-\text{CH}_4$ environment, naphthalene undergoes only 10% conversion, with the majority of the products

Table 5. Major Products from –20 Mesh DECS 19 Pyrolysis under Inert versus Reactive Environments at 1000 and 1 °C/ms

Argon		50% CH ₄ –50% argon		50% H ₂ –50% argon		25% H ₂ –25% CH ₄ –50% argon	
major product species	% conc. excluding unreacted species	major product species	% conc. excluding unreacted species	major product species	% conc. excluding unreacted species	major product species	% conc. excluding unreacted species
benzene	4.75	benzene	8.63	benzene	6.88	benzene	6.59
toluene	9.92	toluene	11.11	toluene	9.56	toluene	9.75
xylene	6.0	xylene	4.77	xylene	6.13	xylene	5.26
methyl-anthracene	4.05	methyl-anthracene	2.55	methyl-anthracene	5.42	methyl-anthracene	4.07
chrysene	2.56	chrysene	1.28	chrysene	2.23	chrysene	2.14
methyl-naphthalene	4.66	methyl-naphthalene	4.9	methyl-naphthalene	5.32	methyl-naphthalene	4.98
methyl-fluoranthene	3.27	methyl-fluoranthene	3.46	methyl-fluoranthene	1.68	methyl-fluoranthene	3.68
methylene-indene	2.73	naphthalene	4.24	methylene-indene	4.37	methylene-indene	3.8
dimethyl-naphthalene	2.27	dimethyl-naphthalene	1.04	dimethyl-naphthalene	1.26	dimethyl-naphthalene	1.25
phenanthrene	2.28	phenanthrene	2.36	phenanthrene	2.97	phenanthrene	2.67
ethylbenzene	1.67	ethylbenzene	1.7	fluorene	2.76	fluorene	2.31

Figure 3. (a) Extent of thermal cracking in Ar and (b) extent of model compounds reacted in Ar–CH₄ at 1000 °C in PFR.Table 6. Major Products of Naphthalene in the Ar–CH₄ Environment from CHEMKIN Simulations

major product species	% conc. in product excl. unreacted species
H ₂	57.9
C ₂ H ₄	7.4
C ₂ H ₆	3.4
C ₄ H ₄	1.3
Benzene	1.6
Methylnaphthalene	26.1

Table 7. Major Products of the Benzene Reaction in the Ar–CH₄ Environment from CHEMKIN Simulations

major product species	% conc. in product excl. unreacted species
H ₂	59.6
C ₂ H ₂	0.3
C ₂ H ₄	18.3
C ₂ H ₆	11.4
Toluene	8.4

consisting of light gases primarily formed through cracking reactions. The upgradation to methylnaphthalene accounts for a mere 2.5% of the overall product composition. The upgradation of all other PAHs in a reactive environment was observed to be

Table 8. Major Products of the Toluene Reaction in the Ar–CH₄ Environment from CHEMKIN Simulations

major product species	% conc. in product excl. unreacted species
H ₂	61.3
C ₂ H ₂	2.1
C ₂ H ₄	15.9
C ₂ H ₆	6.9
Benzene	3.9
Styrene	4.1
Anthracene	1.9
Xylene	0.3

Table 9. Major Products of Toluene Reaction in a Pure Ar Environment from CHEMKIN Simulations

major product species	% conc. in product excl. unreacted species
H ₂	53.6
CH ₄	10.8
C ₂ H ₂	4.2
C ₂ H ₄	1.0
C ₆ H ₆	12.3
Styrene	1.1

Table 10. Major Products of Toluene in the Ar–H₂ Environment from CHEMKIN Simulations

major product species	% conc. in product excl. unreacted species
CH ₄	45.1
C ₂ H ₄	2.7
C ₂ H ₆	1.7
Benzene	45.0
Anthracene	2.3

even lower (not shown here), with their primary product being light gases, resembling the reaction observed in an inert environment (Tables 7–9).

3.3. Assessing Potential Graphitic Quality Improvement with Model Compounds. The graphitic quality, as gauged by stacking height L_c and in-plane crystallite size L_a , of graphitized methylated compounds was significantly higher than their nonmethylated counterparts. Figure 4 shows overlaid XRD plots for graphitized model compounds, and the inset shows the 002 peak profile. The smaller fwhm's in methylated compounds indicate better stacking of the graphitic planes, while their similar peak positions indicate comparable interplanar spacing. Table 11 shows lattice parameters extracted from XRD deconvolution for model compounds. GR-methylnaphthalene and GR-methylanthracene showed 125 and 18% improvement in L_a , while L_c increased by ~37% for both.

TEM images revealed that graphitized samples had flake morphology, as shown in Figure 5. HRTEM of GR-naphthalene and GR-methylnaphthalene confirmed that methylated samples had much larger stacking heights and lateral dimensions of graphene layers. On the other hand, nonmethylated samples possessed smaller crystallites with lamellae curvature and a wavy nanostructure, surrounded by amorphous carbon regions. SAED patterns for methylated samples showed sharp diffraction rings as compared to confirmed diffuse rings for nonmethylated samples, confirming the better crystallinity.

3.4. Color Appearance of Pure versus cMW-Upgraded Products. Transparent colorless benzene turned into different yellowish shades after reacting in different MW plasma environments, as shown in Figure 6. The ap-benzene looks nearly the same in color as pure benzene (colorless), with a very small tinge of yellow. On the other hand, hp-benzene and mp-

benzene are clearly yellowish liquids, with the latter being slightly darker yellow. The absorption of light indicates that these products contain molecules with higher conjugation compared to pure benzene. This suggests that MW plasma containing reactive gases H₂ and CH₄ promotes concatenation and/or olefinic addition to the aromatics.

3.5. Analysis of Plasma-Reacted Products. Figure 7 shows total ion chromatograms of products obtained from the reaction of benzene under different MW plasma environments, and Table 12 summarizes the major components found in each sample. Profound differences were found between the products from different MW plasma environments. The ap-benzene contained primarily concatenation products such as azulene, indene, biphenyl, etc. In the presence of reactive MW plasma, both concatenation and products with substantially higher H/C ratios were achieved. The mp-benzene contains hydrogenated products such as methylcyclohexane along with condensation products such as chrysene, naphthalene, and biphenyl. The hp-benzene showed alkylation products such as toluene and ethylbenzene, along with concatenation products such as terphenyl, naphthalene, and biphenyl. The reactive MW plasma produces hydrogenated and alkylated products with an overall significant H/C compared to the argon MW plasma.

3.6. Graphitic Quality Comparison between GR-Pure versus MW-Upgraded Products. Figure 8 shows the XRD overlays of graphitized benzene coke versus MW plasma-upgraded products, and the inset shows an overlay of their 002 peaks. Table 13 shows the XRD-derived crystallite lattice parameters using Scherrer's equation on fitted peaks. Benzene reacted in Ar plasma showed very little improvement over that of pure benzene after graphitization. But the products from reactive plasma environments showed substantial improvements in graphitic quality over pure benzene after graphitization. The narrower full width at half-maximum (fwhm) is clearly visible for GR-hp-benzene, indicating a larger crystallite size. The in-plane crystallite size increased by more than 90%, and the stacking height increased by around 70% in GR-hp-benzene compared to GR-benzene. The improvements observed for products that reacted in CH₄ plasma were yet more remarkable. Very sharp and narrow diffraction peaks were observed for GR-mp-benzene, indicating that the average crystallite size is very large and vastly different compared to GR-benzene. A notable

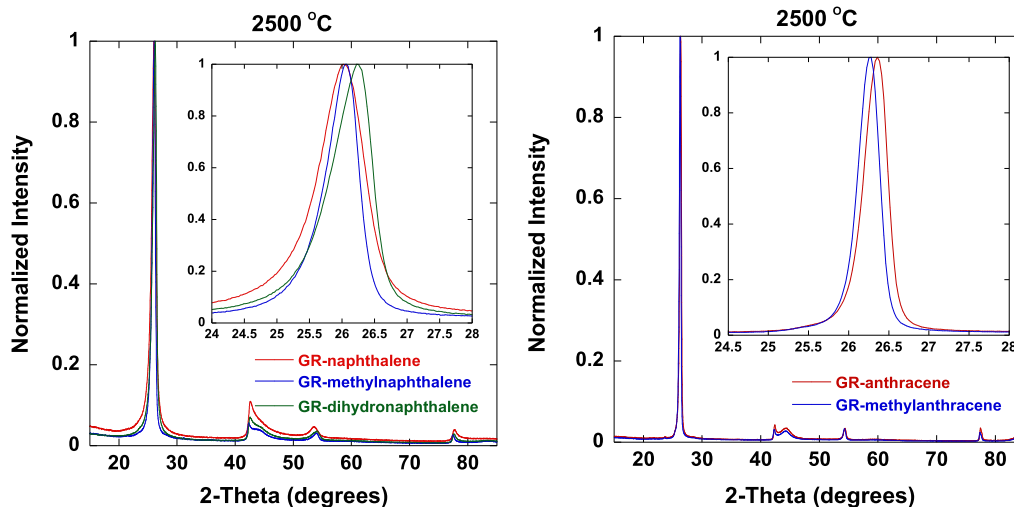


Figure 4. XRD overlays of graphitized model compounds.

Table 11. XRD-Derived Lattice Parameters for Graphitized Model Compounds

lattice parameter compound	GR-naphthalene	GR-dihydronaphthalene	GR-methylnaphthalene	GR-anthracene	GR-methylanthracene
d_{002} [Å]	3.412	3.39	3.395	3.391	3.395
L_c (using 002) [nm]	9.9	11.4	13.5	20.0	27.2
L_a (using 100) [nm]	7.4	14.7	28.3	37.4	48.0
L_a (using 110) [nm]	21.8	35.3	49.0	68.0	80.3

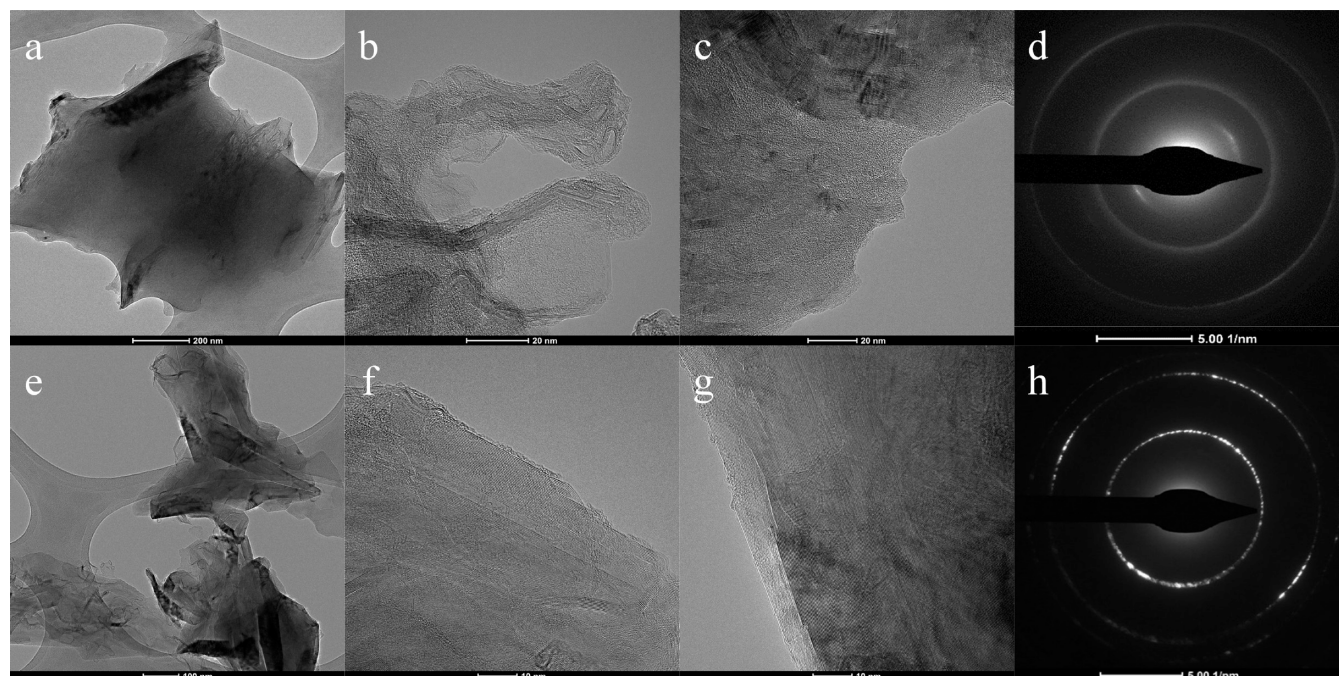


Figure 5. TEM images of GR-naphthalene showing (a) morphology, (b,c) nanostructure, (d) SAED pattern, versus TEM images of GR-methylnaphthalene showing (e) morphology, (f,g) nanostructure, and (h) SAED pattern.

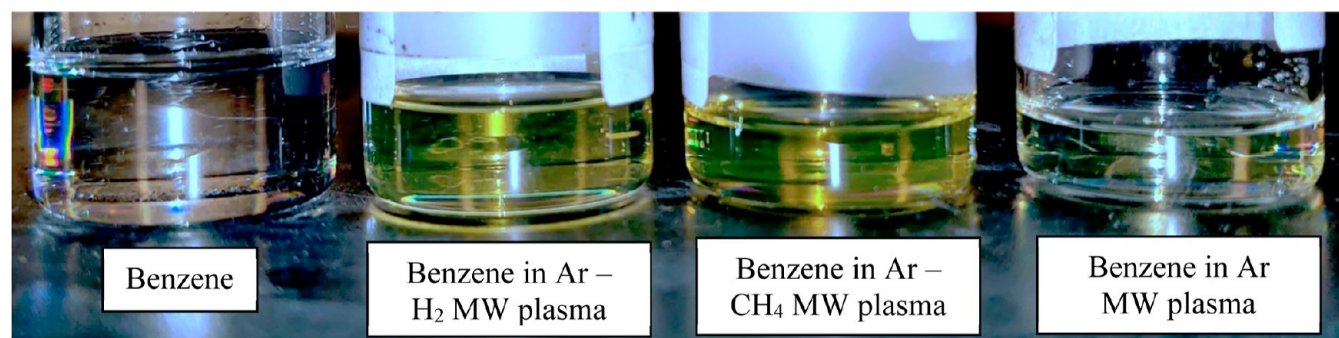


Figure 6. Color appearance of benzene vs products obtained from the reaction of benzene in different MW plasma environments.

shift in the 002 peak position shows that the interplanar spacing between the graphitic planes has reduced markedly. This, along with the noticeable emergence of hkl lines in XRD, signifies a great improvement of crystalline order in the third (*c*-axis) direction. Compared to GR-benzene, GR-mp-benzene showed L_a and L_c increases of 650 and 370%, respectively.

Figures 9 and 10 show panels of TEM images of GR-benzene and GR-ap-benzene, respectively. The nanostructure of GR-ap-benzene was very similar to that of GR-benzene, confirming the XRD analysis. Their nanostructure consisted of very short crystallites with extensive lamellar curvature and intertwining. A few stacks of ~ 10 nm long lamellae were observed, along with some nongraphitic shells and amorphous fringes.

Figure 11 shows a panel of TEM images of GR-hp-benzene. The graphitic quality improvement is evidenced by a dramatic reduction in the lamellar curvature and amorphous nanostructure. In contrast to the shells and intertwined ribbons formed by graphene stacks and pore walls observed in GR-benzene, GR-hp-benzene exhibits a flakelike morphology characterized by contiguous lamellae exceeding 20 nm in length. Although some intertwining still exists, the individual lamellae stacks are easily distinguishable, and the stacking height is significantly larger. Figure 12 shows the TEM images for GR-mp-benzene. GR-mp-benzene produced highly graphitic flakes with little to no lamellar cross-links and curvature. Well-stacked contiguous lamellae larger than 50 nm were observed in all the surveyed flakes/particles.

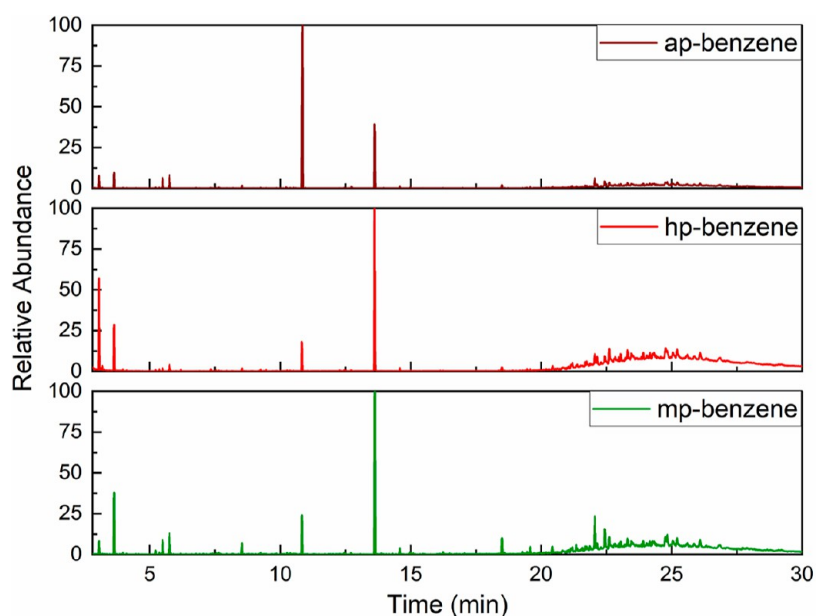
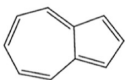
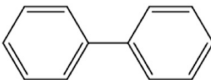
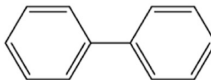
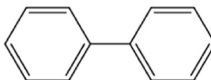
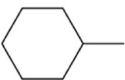
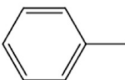
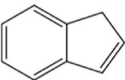
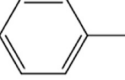
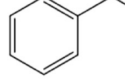
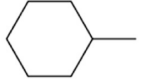
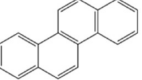
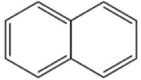
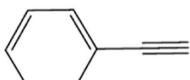
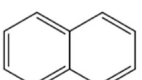
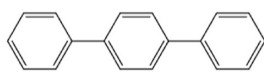


Figure 7. Total ion chromatograms of products obtained from the reaction of benzene in different MW plasma environments.

Table 12. Major Products Obtained from the Reaction of Benzene under Different MW Plasma Environments

ap-benzene major product species	Relative abundance (%)	hp-benzene major product species	Relative abundance (%)	mp-benzene major product species	Relative abundance (%)
Azulene 	58.3	Biphenyl 	43.6	Biphenyl 	35.7
Biphenyl 	17.8	Methylcyclohexane 	23.7	Toluene 	23.1
Indene 	3.5	Toluene 	10	Ethylbenzene 	17.7
Methylcyclohexane 	2.3	Chrysene 	8.7	Naphthalene 	8.8
Phenylethyne 	2.1	Naphthalene 	8.3	Terphenyl 	8.7

4. DISCUSSION

The fast pyrolysis using py-GC-MS shows that small changes in the particle size and temperature ramp rates did not have a significant effect on the thermal devolatilization of coals. Limited plasma pyrolysis studies conducted previously could not clearly answer to what extent the high-temperature thermal effects aid

or hinder plasma action. Thermal pyrolysis under reactive gases did not assist coal matrix deconstruction and also did not lead to significant upgrading of the evolved volatiles. This is because the reactive gases undergo very little thermal dissociation, as shown by chemical kinetic simulations, and therefore, the evolved volatiles have a propensity to crack rather than get upgraded by reaction with the reactive gases. This necessitates a plasma to

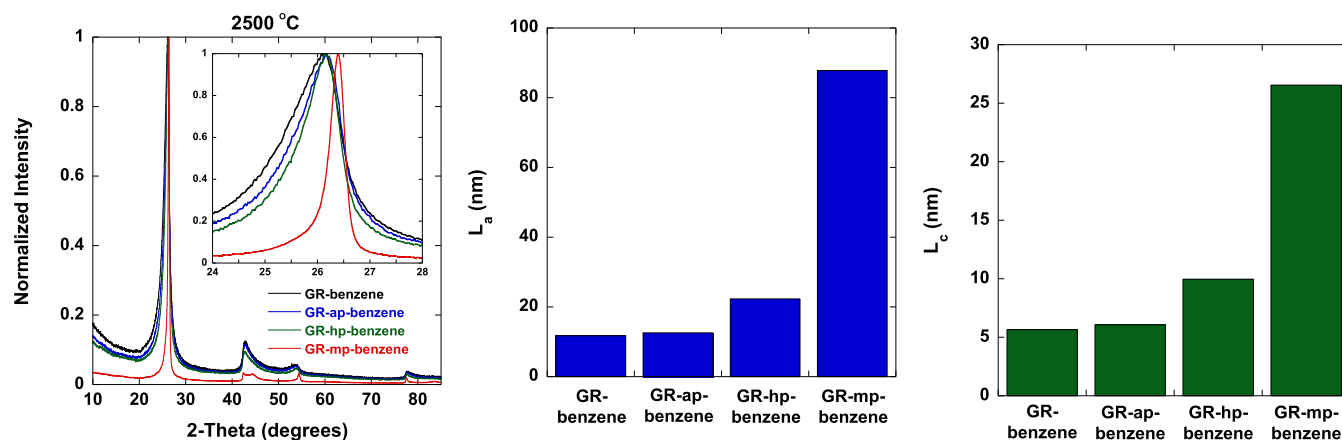


Figure 8. XRD overlays of graphitized benzene coke vs MW plasma-upgraded products.

Table 13. XRD-Derived Lattice Parameters for Graphitized Benzene Coke versus MW Plasma-Upgraded Products

lattice parameter sample	GR-benzene	GR-ap-benzene	GR-hp-benzene	GR-mp-benzene
d_{002} [Å]	3.404	3.40	3.396	3.372
L_c (using 002) [nm]	5.65	6.06	9.96	26.54
L_a (using 100) [nm]	7.70	8.81	9.01	25.75
L_a (using 110) [nm]	11.74	12.61	22.31	87.82

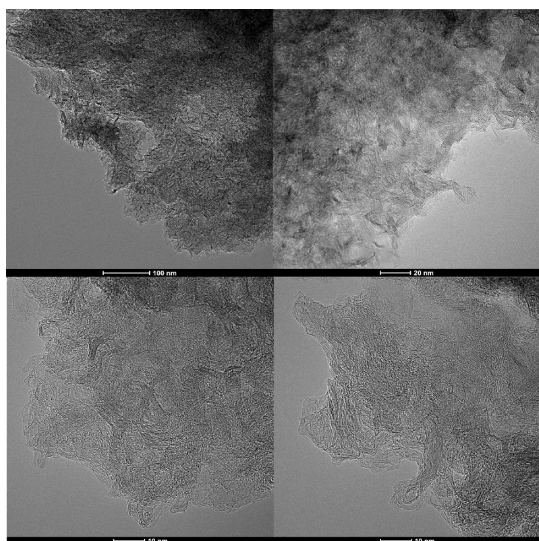


Figure 9. TEM images of GR-benzene coke.

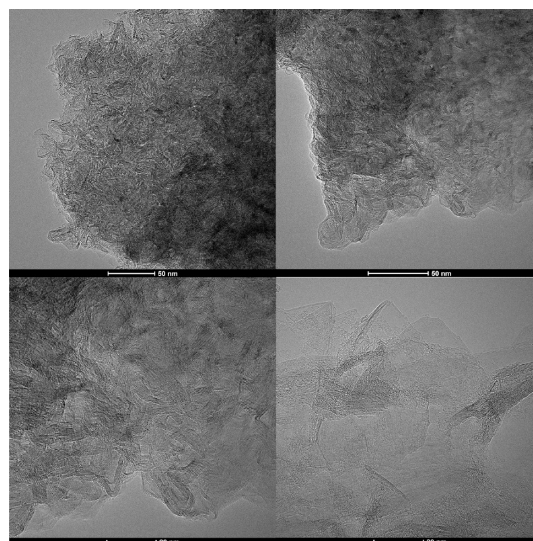


Figure 10. TEM images of GR-ap-benzene coke.

help provide radicals from the reactive gas for upgrade to occur. These tests provide an important benchmark for the MW plasma pyrolysis tests, as any upgrade observed in those can be interpreted as a result of plasma effects, namely, the radical capping reactions without thermal contribution.

Indeed, the MW plasma was found to be very effective in upgrading the products by increasing their H/C content. The reaction of benzene in reactive MW plasma environments produces yellowish products, indicating concatenation and/or olefinic addition to the aromatics. This theory was further confirmed by GC–MS analysis of condensed products obtained from the reaction of benzene under different MW plasma environments. Products from nonreactive argon MW plasma predominantly contained concatenation precursors, whereas MW plasma containing hydrogen and methane produced hydrogenated and methylated precursors with substantially higher H/C. The MW plasma efficiently generates H and CH₃

radicals from reactive gases (H₂ and CH₄), which then undergo reactions with benzene, including ring opening and radical capping, resulting in the production of upgraded precursors.

GR-benzene produced very small crystallites around 12 nm long lamellae with a 5 nm stacking height. GR-ap-benzene did not show substantial improvement in crystallite sizes over GR-benzene despite concatenation reactions. This could be because ap-benzene contained aromatics with nonhexagonal rings such as azulene and indene, which have been shown to induce curvature in lamellae,^{38,39} thus inhibiting the development of stacked, parallel lamellae. On the other hand, precursors that were upgraded from reactive MW plasma exposure exhibited significantly improved graphitic quality following HT. The 002 peaks were symmetric and corresponded to a single uniform sp² carbon phase. The hp-benzene containing hydrogenated precursors led to substantially larger crystallites after graphitization, with L_a and L_c being larger by more than 70%. The MW

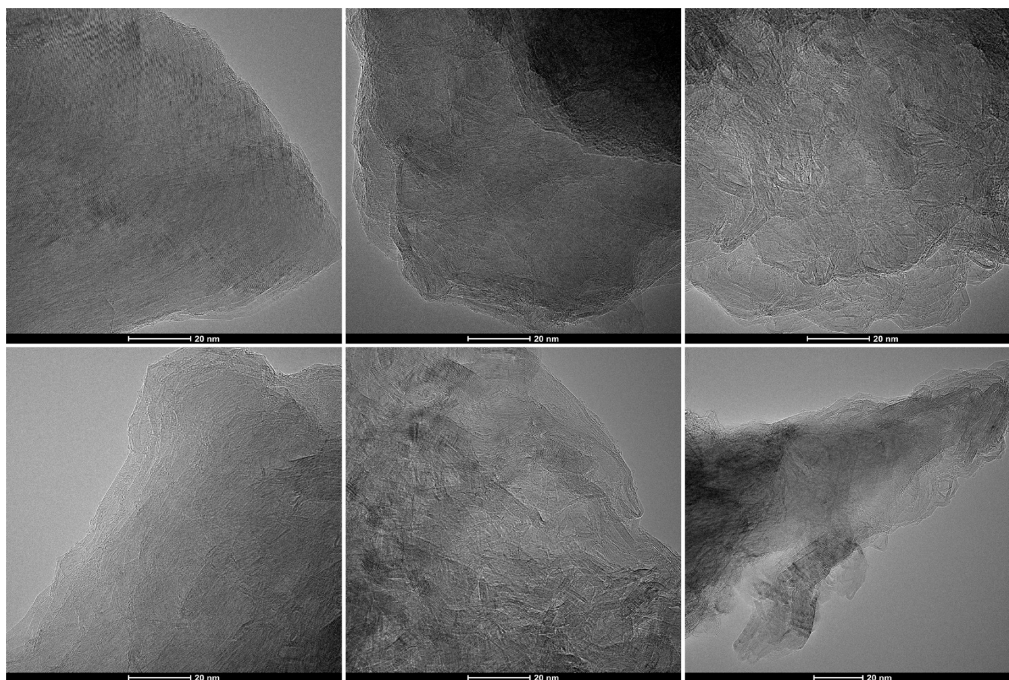


Figure 11. TEM images of GR-hp-benzene coke.

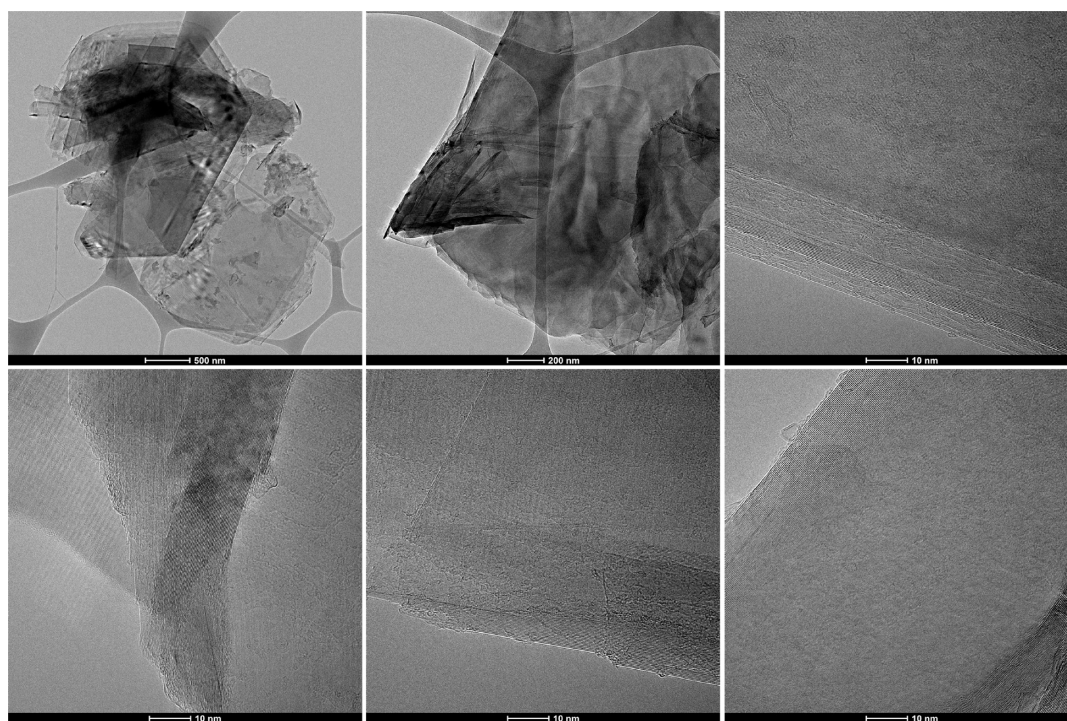


Figure 12. TEM images of the GR-mp-benzene coke.

plasma containing methane was much more effective in upgrading the precursor and produced crystallites several folds larger compared to pure benzene after graphitization. GR-mp-benzene has L_a and L_c larger than GR-benzene by 650 and 370%, respectively. Benzene, which does not form a very good mesophase, transformed into a precursor as good as pitch⁴⁰ after upgradation in methane MW plasma. These upgraded precursors produce high-quality products with large stacks of contiguous lamellae with minimum curvature and cross-linking. Interestingly, the study of graphitization of model compounds

also showed similar results with a huge potential for improving graphitic quality by upgrading precursors. Methylation was found to be more effective than hydrogenation in improving the graphitic quality in the model compounds. The limitation of this study is that MW plasma tests were performed on benzene as a model compound, whereas coal devolatilization generates a diverse range of compounds that may exhibit varying behaviors or similar behaviors to varying degrees. The challenge of the MW plasma pyrolysis of coal on a large scale needs to be evaluated.

5. CONCLUSIONS

This work compares the effectiveness of conventional thermal pyrolysis versus reactive MW plasma pyrolysis for upgrading precursors obtained from coal. The thermal pyrolysis results indicate that thermal pyrolysis is ineffective in facilitating the upgrading of devolatilized products, highlighting the necessity for an alternative approach. Reaction in a nonreactive argon MW plasma primarily produces concatenated precursors, but it does not produce a significant improvement in graphitic quality after HT, likely due to the presence of nonhexagonal rings in the aromatic products. Reactive MW plasma pyrolysis, on the other hand, produced upgraded products with significantly higher H/C, which led to higher graphitic quality products after HT. MW plasma containing both reactive gases (hydrogen and methane) showed hydrogenation and alkylation along with concatenation. This upgrade increased the graphitic quality of heat-treated liquid products by several folds. By employing MW plasma containing methane, poorly graphitizable precursors such as benzene were transformed into a precursor mixture that exhibited a graphitic quality comparable to CT pitch. In summary, increasing the H/C ratio by methylation or hydrogenation of the precursors substantially improves the graphitic quality of the heat-treated products. This study successfully demonstrates the potential of MW plasma for obtaining upgraded precursors.

AUTHOR INFORMATION

Corresponding Author

Akshay Gharpure – John and Willie Leone Family Department of Energy and Mineral Engineering and the EMS Energy Institute, Penn State University, University Park, Pennsylvania 16802, United States; orcid.org/0000-0001-8823-3949; Email: apg86@psu.edu

Author

Randy L. Vander Wal – John and Willie Leone Family Department of Energy and Mineral Engineering and the EMS Energy Institute, Penn State University, University Park, Pennsylvania 16802, United States; orcid.org/0000-0002-5847-9726

Complete contact information is available at:
<https://pubs.acs.org/10.1021/acsomega.3c05382>

Notes

The authors declare no competing financial interest.

ACKNOWLEDGMENTS

Acknowledgment is made to the donors of the American Chemical Society Petroleum Research Fund for support of this research.

REFERENCES

- (1) Kumar, S.; Anderson, D. P.; Crasto, A. S. Carbon Fibre Compressive Strength and Its Dependence on Structure and Morphology. *J. Mater. Sci.* **1993**, *28* (2), 423–439.
- (2) Wang, M. L.; Bian, W. F. The Relationship between the Mechanical Properties and Microstructures of Carbon Fibers. *N. Carbon Mater.* **2020**, *35* (1), 42–49.
- (3) Johnson, D. J. Structure/Property Relationships in Carbon Fibres. *J. Phys. D Appl. Phys.* **1987**, *20*, 286.
- (4) Li, D.; Wang, H.; Wang, X. Effect of Microstructure on the Modulus of PAN-Based Carbon Fibers during High Temperature

- Treatment and Hot Stretching Graphitization. *J. Mater. Sci.* **2007**, *42* (12), 4642–4649.
- (5) Newcomb, B. A. Processing, Structure, and Properties of Carbon Fibers. *Composites, Part A* **2016**, *91*, 262–282.
- (6) Balandin, A. A. Thermal Properties of Graphene and Nanostructured Carbon Materials. *Nat. Mater.* **2011**, *10* (8), 569–581.
- (7) Klein, C. A. Electrical Properties of Pyrolytic Graphites. *Rev. Mod. Phys.* **1962**, *34* (1), 56–79.
- (8) Zabihi, O.; Shafei, S.; Fakhrohoseini, S. M.; Ahmadi, M.; Ajdari Nazarloo, H.; Stanger, R.; Anh Tran, Q.; Lucas, J.; Wall, T.; Naebe, M. Low-Cost Carbon Fibre Derived from Sustainable Coal Tar Pitch and Polyacrylonitrile: Fabrication and Characterisation. *Materials* **2019**, *12* (8), 1281.
- (9) Nippon Steel News. Pitch-based Carbon Fiber. 2020, <https://www.nipponsteel.com/en/company/publications/monthlynsc/pdf/2011021411272812861.pdf> (accessed Nov 2, 2020).
- (10) Song, C.; Schobert, H. H. Non-Fuel Uses of Coals and Synthesis of Chemicals and Materials. *Fuel* **1996**, *75* (6), 724–736.
- (11) Song, C.; Schobert, H. H. Opportunities for Developing Specialty Chemicals and Advanced Materials from Coals. *Fuel Process. Technol.* **1993**, *34* (2), 157–196.
- (12) MarketWatch. *Coke Market Size By Regional Industry Growth, Statistics & Forecast*, 2019.
- (13) Krainik, C. E. Strategies for a Declining North American Coal Tar Supply. *National Coal Industrial Meeting, Ohio, US*, 2005.
- (14) Mark Morris. How is Crude Coal Tar Derived?. 2020, http://www.truthaboutcoaltar.com/pdf/How_is_Crude_Coal_Tar_Derived.pdf (accessed Aug 2, 2020).
- (15) Osman, A. I.; Farghali, M.; Ihara, I.; Elgarahy, A. M.; Ayyad, A.; Mehta, N.; Ng, K. H.; Abd El-Monaem, E. M.; Eltaweil, A. S.; Hosny, M.; Hamed, S. M.; Fawzy, S.; Yap, P. S.; Rooney, D. W. *Materials, Fuels, Upgrading, Economy, and Life Cycle Assessment of the Pyrolysis of Algal and Lignocellulosic Biomass: A Review*; Springer International Publishing, 2023; Vol. 21.
- (16) Bermúdez Menéndez, J. M.; Beneroso Vallejo, D.; Rey Raap, N.; Arenillas de la Puente, A.; Menéndez Diaz, J. A. Energy Consumption Estimation in the Scaling-up of Microwave Heating Processes. *Energy Consumption Estimation in the Scaling-up of Microwave Heating Processes*; Elsevier, 2015.
- (17) Solomon, P. R.; Serio, M. A.; Suuberg, E. M. Coal Pyrolysis: Experiments, Kinetic Rates and Mechanisms. *Prog. Energy Combust. Sci.* **1992**, *18* (2), 133–220.
- (18) Durai-Swamy, K. Pyrolysis process for producing condensed stabilized hydrocarbons utilizing a beneficially reactive gas. U.S. Patent 4,324,642 A, 1982.
- (19) Xu, W. C.; Tomita, A. Effect of Coal Type on the Flash Pyrolysis of Various Coals. *Fuel* **1987**, *66* (5), 627–631.
- (20) Tramp, P. J. J. *Coal Pyrolysis: Basic Phenomena Relevant to Conversion Process*; University of Amsterdam, 1987.
- (21) Akhtar, J.; Saidina Amin, N. A Review on Operating Parameters for Optimum Liquid Oil Yield in Biomass Pyrolysis. *Renew. Sustain. Energy Rev.* **2012**, *16* (7), 5101–5109.
- (22) Chakrabarty, S. K.; Du Plessis, M. P. *Modern Coal Pyrolysis. A State-of-the-Art Review*; U.S. Department of Energy, 1982.
- (23) Gibbins-matham, J.; Kandiyoti, R. Coal pyrolysis yields from fast and slow heating in a wire-mesh apparatus with a gas sweep. *Energy Fuels* **1988**, *2* (4), 505–511.
- (24) Binner, E.; Lester, E.; Kingman, S.; Dodds, C.; Robinson, J.; Wu, T.; Wardle, P.; Mathews, J. P. A Review of Microwave Coal Processing. *J. Microw. Power* **2014**, *48*, 35–60.
- (25) Zuo, H.; Long, S.; Wang, C.; Zhang, P. A Review of Microwave Treatment on Coal. *7th International Symposium on High-Temperature Metallurgical Processing*; Springer, 2016; pp 617–624.
- (26) Pickles, C. A.; Gao, F.; Kelebek, S. Microwave Drying of a Low-Rank Sub-Bituminous Coal. *Miner. Eng.* **2014**, *62*, 31–42.
- (27) Lester, E.; Kingman, S. The Effect of Microwave Pre-Heating on Five Different Coals. *Fuel* **2004**, *83* (14–15), 1941–1947.
- (28) Mingjie, X. H. L. Q. M.; Jienan, P. Application of microwave in coal processing and utilization. *Coal Convers.* **2012**, *1*, 86–89.

- (29) Griffin, T. P.; Howard, J. B.; Peters, W. A. An Experimental and Modeling Study of Heating Rate and Particle Size Effects in Bituminous Coal Pyrolysis. *Energy Fuels* **1993**, *7* (2), 297–305.
- (30) Fu, Y. C.; Blaustein, B. D. Pyrolysis of Coals in a Microwave Discharge. *Ind. Eng. Chem. Process Des. Dev.* **1969**, *8* (2), 257–262.
- (31) Singh, S.; Neculaes, V. B.; Lissianski, V.; Rizeq, G.; Bulumulla, S. B.; Subia, R.; Manke, J. Microwave Assisted Coal Conversion. *Fuel* **2015**, *140*, 495–501.
- (32) Yang, K.; Batts, B. D.; Wilson, M. A.; Martin, L.; Maa, P. S.; Long, M. A.; He, S. X. J.; Attalla, M. I. Reaction of Methane with Coal. *Fuel* **1997**, *76* (12), 1105–1115.
- (33) Kamei, O.; Onoe, K.; Marushima, W.; Yamaguchi, T. Brown Coal Conversion by Microwave Plasma Reactions under Successive Supply of Methane. *Fuel* **1998**, *77* (13), 1503–1506.
- (34) Rahimi, P.; Fairbridge, C.; Tanner, D. D. The Use of Methane as Source of Higher Hydrocarbons and Hydrogen for Upgrading Heavy Oils and Bitumen. *Prepr. Pap.—Am. Chem. Soc., Div. Fuel Chem.* **1998**, *43* (3), 476–480.
- (35) Davis, A.; Glick, D. C.; Hatcher, P. G.; Mitchell, G. D. *Maintenance of the Coal Sample Bank & Database*, 11/99, 2841095, 1999.
- (36) Saggese, C.; Ferrario, S.; Camacho, J.; Cuoci, A.; Frassoldati, A.; Ranzi, E.; Wang, H.; Faravelli, T. Kinetic Modeling of Particle Size Distribution of Soot in a Premixed Burner-Stabilized Stagnation Ethylene Flame. *Combust. Flame* **2015**, *162* (9), 3356–3369.
- (37) Ranzi, E.; Frassoldati, A.; Grana, R.; Cuoci, A.; Faravelli, T.; Kelley, A. P.; Law, C. K. Hierarchical and Comparative Kinetic Modeling of Laminar Flame Speeds of Hydrocarbon and Oxygenated Fuels. *Prog. Energy Combust. Sci.* **2012**, *38* (4), 468–501.
- (38) Kumal, R. R.; Liu, J.; Gharpure, A.; Vander Wal, R. L.; Kinsey, J. S.; Giannelli, B.; Stevens, J.; Leggett, C.; Howard, R.; Forde, M.; Zelenyuk, A.; Suski, K.; Payne, G.; Manin, J.; Bachalo, W.; Frazee, R.; Onasch, T. B.; Freedman, A.; Kittelson, D. B.; Swanson, J. J. Impact of Biofuel Blends on Black Carbon Emissions from a Gas Turbine Engine. *Energy Fuels* **2020**, *34*, 4958–4966.
- (39) Gharpure, A.; Vander Wal, R. Improving Graphenic Quality by Oxidative Liberation of Crosslinks in Non-Graphitizable Carbons. *Carbon* **2023**, *209* (April), 118010.
- (40) Gharpure, A.; Vander Wal, R. L.; Pisupati, S. Synthetic Pitch from Solvent Extraction of Coal as a Source for High-Quality Graphite. *C* **2023**, *9* (2), 56.